Scientia Iranica A (2022) 29(6), 2919–2939

Sharif University of Technology
Scientia Iranica
Transactions A: Civil Engineering
http://scientiairanica.sharif.edu

Fragility analysis of RC bridges considering spatially varying ground motions and SSI

A. Hosseinnezhad and A. Gholizad*

Department of Civil Engineering, University of Mohaghegh Ardabili, Ardabil, Iran.

Received 3 April 2021; received in revised form 30 December 2021; accepted 25 April 2022

KEYWORDS
Spatially varying ground motions;
Wave-passage;
Incoherence;
Site-response;
Fragility curves.

Abstract. Long-span structures like bridges experience different movements at the supports because of the wave-passage, incoherence, and site-response effects. In this study, spatially varying ground motions were used to evaluate the seismic vulnerability of different RC bridges. To this end, three prototype Caltrans reinforced concrete curve bridges with different column heights and radii were selected and used for the numerical study. The spatially correlated ground motions were generated by the conditional simulation method and then, were converted into corresponding displacement time histories to perform non-uniform excitations. The structures were analyzed under generated series, and the fragility curves were developed based on the defined limit states. Furthermore, soil-structure interactions and different soil conditions were included in evaluating the non-linear behavior of the bridges. The results show that the damage exceedance probability increased under non-uniform excitations and it is more evident for long-span bridges. Also, it is found that the effect of soil-structure interactions on the probability of failure of short-span bridges is negligible and the impact is still significant for long-span bridges. Moreover, based on the results for structures situated on soft deposits, the combination of spatially varying ground motions in conjunction with soil-structure interactions remarkably increases the responses.

1. Introduction

Three decades ago, the issue of non-uniform excitation of long-span structures had been of concern for the structural and earthquake engineering community. The main reason for non-uniform excitations is the spatially varying ground movements. An overview of the bridge design codes reveals that most of them ignore the issue of non-uniform excitations, as previous studies have shown that the effect of spatially varying ground motions on the structures in several cases was too destructive [1]. Since 1980, numerous related studies have been accomplished and valuable papers came out. Most of these papers have used deterministic approaches to investigate the behavior of structures under non-uniform excitations, and the probabilistic methods have received less attention. Since the dynamic response of structures is closely related to the frequency content of the excitation records and the frequency characteristics of the desired structure, the application of deterministic methods cannot accurately reflect the seismic behavior of the structures [2]. By using the probabilistic methods, the issue will be resolved. Nowadays, probabilistic methods are implemented as a convenient tool for the risk reduction in the case of structures [3–6]. One of the best ways to assess risk for a given structure is to produce the corresponding

*. *Corresponding author.*
E-mail address: Gholizad@uma.ac.ir (A. Gholizad)

doi: 10.24200/sci.2022.58039.5533

fragility curves [7–19]. Fragility curves are conditional interpretations that present the probability of exceeding a structure through a pre-defined limit state under a given intensity measure [20]. Deterministic approaches were extensively utilized for generating the fragility curves. Mangalathu et al. (2018) studied the seismic vulnerability of horizontally curved bridges constructed in California. They surveyed how the column height and deck curvature could affect the fragility of the bridges. For a numerical study, several existing bridges were selected and the finite element models were analyzed under different time histories. They found that increasing the deck curvature would adversely affect the safety of the bridge. Also, for bridges with tall piers designed before 1970, the results revealed that increasing the piers height led to lower safety standards [21]. Xie and DesRoches (2019) investigated the relation between soil-structure interaction parameters and the fragility of bridges. The results showed that the bridge efficiency and fragility curves of bridge columns and decks were dominated by uncertainty in the ground motion [22]. Noori et al. (2019) studied the effects of ground motions directionality on the seismic behavior of skewed bridges. They included soil-structure interactions and considered twelve different incident angles. The results showed that the critical incident angle did not necessarily coincide with the main axes of the structure [23]. Chen (2020) studied the seismic fragility of an entire reinforced concrete tall-pier bridge under near-fault ground motions in China. The probabilistic demand models are made based on the results of time history analysis and the fragility curves constructed for components and system level. The results revealed that for bridges with tall piers, the system fragility was predominant compared to the components level [24]. Shekhar et al. (2020) perused the evolution of seismic design codes in recent decades. They analyzed different types of bridges and designed those under different seismic considerations. Also, non-linear finite element models were developed to simulate different types of failure. The results showed that the seismic behavior of bridges designed based on revised codes improved remarkably [25]. In another study by Wei et al. (2021), a tall three-tower cable-stayed bridge was analyzed to evaluate the seismic sensitivity for different soil conditions. They used the OpenSees platform to establish a finite element model. Then, the required time series were generated based on the corresponding site response spectrum. The results showed that the soft soil condition increased the probability of failure [26]. Rachedi et al. (2021) studied the fragility of a bridge using artificial neural networks considering soil-structure interactions. They formed a verified database from a finite element model to train a neural network. Then, the bridge was analyzed under generated time series and the fragility curves developed. The results proved considering the soil-structure interactions to be very important in evaluating the probability of failure [27]. Salimi et al. (2021) investigated the seismic behavior and fragility of circular and rectangular cross-section reinforced concrete columns under multi-directional excitations. They surveyed the different failure scenarios of the columns under various excitations. The outcomes represented that the multiple excitations of the column significantly increased the rate of damages. Also, they found that the rectangular sections were more vulnerable than circular cross-sections [28]. Todorov and Muntasir Billah (2021) studied the seismic behavior of a bridge pier for different types of excitations. They analyzed the bridge under near-fault, far-field, and long-duration excitations. For a numerical study, a non-linear fiber-based finite element model of a real seismically designed bridge was used to evaluate the probability of failure under different ground motions. They found that the current design guidelines do not include the duration of ground motions and pulse effects [29]. Fosoul Saber and Tait Michael (2021) investigated the seismic vulnerability of several retrofitted bridges established before 1970. They developed finite element models for each bridge and excited them under 40-time series. The study revealed that the elastomer components used for retrofitting the bridge favorably decreased the shear forces transferred to the bridge column. Also, they found that the elastomer component would adversely affect the safety of abutments in the longitudinal direction [30]. However, the evaluation of the fragility in the studies was mentioned above and many similar studies have been done under the assumption of uniform or deterministic excitation; therefore, the results may not be exact because of variations in the characteristics of traveling waves [31]. In long-span structures, because of changes in seismic traveling waves, each support experiences different movements during an earthquake. Therefore, it is essential to include the spatial variations of ground motions in developing fragility curves [32]. On the other hand, studies on the effect of spatially varying ground motions on long structures have paid little attention to the issue of fragility curves. In recent years, significant studies have been conducted on the effects of spatial varying of ground movements on long structures [33–37]; still, none of them has investigated the effects of spatial varying ground motions on the fragility of structures. From the past studies, since the issue of probabilistic seismic risk assessment of bridges due to spatially varying ground motions with effects of soil-structure inter-actions has received less attention, an attempt has been made in the current research to investigate the mentioned issue of the fragility of structures. Therefore, the structural failure due to spatially varying ground movements was examined and compared with the same results from

uniform excitation. In addition, the effect of changes in site conditions on seismic responses of structures was explored. For this purpose, different soil conditions were considered and the effects of soil-structure interaction were discussed. For numerical studies, a horizontal curved reinforced concrete bridge, which is very common in California, has been selected and modeled. To investigate a larger range of frequencies, three pier heights, and radius of curvature, a total of nine structures were considered and the finite element model was formed in OpenSees platforms [38]. To perform nonlinear time history analysis for fragility assessment, a set of 100-time series was simulated at supports based on the method introduced by Konakli and Der Kiureghian (2011, 2012) [39,40]. The damage exceedance probability of the bridges was evaluated based on the limit states and the related fragility curves were developed. Each bridge was analyzed for non-uniform and uniform excitations and also, effects of soil-structure interactions were studied in the last section. Given that the number of earthquakes recorded for a given area is usually deficient and, in many cases, rare, it is necessary to simulate the time series needed to perform a time history analysis for a predefined spatially varying model for the region of interest. Although simulated records with this method provide valuable information on the fragility analysis of structures, they are ultimately largely artificial [41]. In return, in the conditional simulation method, generated time series include the specifications of the original records like non-stationarity in soil conditions, amplitude and frequency content, distance from the source-site, and earthquake magnitude. A simulation model was introduced by Konakli and Der Kiureghian (2011, 2012) [39,40] and the wave-passage, incoherence, and site effects were considered. Since it can model all the parameters involved in the spatial variations of seismic waves, it is used in this research.

2. Fragility functions

The current paper implements the seismic demand model and capacity-based boundary conditions to develop fragility curves based on the results of nonlinear dynamic analysis. Fragility can be defined as a conditional probability in which the structural seismic demand (D) for a given level of ground intensity (IM) reaches a maximum capacity value (C). Considering the demand and capacity, both of them follow the log-normal distribution of the fragility introduced as follows:

$$P\left(D \geq C \left| IM \right.\right) = \Phi\left[\frac{\ln\left(S_D\right) - \ln\left(S_C\right)}{\sqrt{\beta^2_{(D|\,IM)} + \beta^2_C}}\right], \tag{1}$$

where $\beta_{(D\,|\,IM)}$ and S_D are dispersion and median value of the demand as a function of IM, respectively; β_C and S_C are dispersion and median of the structural capacity, respectively; and the cumulative normal distribution function is presented by $\Phi[.]$. Eq. (2) defines the demand model [3]:

$$\ln\left(S_D\right) = a.\ln\left(IM\right) + b, \tag{2}$$

where a and b are coefficients of regression and calculated from analysis outputs.

3. Simulation of spatially varying ground motions

This section presents, the conditional method. Considering that time series $[a_k\left(t_i\right)]$ define a time history at location k and assuming that N is even, an estimator of the auto-power spectral density ($auto-PSD$) of the time series is shown as:

$$G_{kk}\left(\omega_p\right) = \frac{N.\Delta t}{4.\pi}\left(A^2_{pk} + B^2_{pk}\right) = \frac{\Delta t}{\pi.N}\left|\sum_{i=1}^{N} a_k\left(t_i\right).\exp\left(i.t_i.\omega_p\right)\right|^2. \tag{3}$$

A_{pk} and B_{pk} are the Fourier factors [40,41]. The $auto-PSDs$ for other desired points are then specified in terms of the evaluated $auto-PSD$ $[G_{kk}(\omega)]$ of the determined time series and Frequency Response Function (FRF) $[H_{kk}(\omega)]$ for the absolute acceleration response of the soil profile for an acceleration input at the bedrock level [39–40].

$$G_{ll}\left(\omega\right) = \frac{G_{kk}\left(\omega\right).\left|H_l\left(\omega\right)\right|^2}{\left|H_k\left(\omega\right)\right|^2}, \tag{4}$$

The *cross-PSD* between locations k and l is given by:

$$G_{kl}\left(\omega\right) = \gamma_{kl}\left(\omega\right).\left[G_{kk}.G_{ll}\left(\omega\right)\right]^{\frac{1}{2}}, \tag{5}$$

where γ_{kl} is the coherency function. Der Kiureghian (1996) [42] introduced a coherency model that considered the incoherence, local site effects, and wave-passage [42,43]. The model is presented as:

$$\gamma_{kl}\left(\omega\right) = \exp\left[-\left(\frac{\alpha\,.\,d_{kl}\,.\,\omega}{\upsilon_s}\right)^2\right].\exp\left[-i\frac{\omega\,.\,d^L_{kl}}{\upsilon_{app}}\right].\exp\left[-i\tan^{-1}\frac{\mathrm{Im}\left[H_k(\omega).H_l(-\omega)\right]}{\mathrm{Re}\left[H_k\left(\omega\right).H_l(-\omega)\right]}\right], \tag{6}$$

where the first term describes the incoherence effects [42,43], second is wave-passage [42], and the third is the site-response effects [39,40]. In this equation, α represents the incoherence, d_{kl} is the distance between stations k and l, υ_s is the shear wave velocity, d^L_{kl} is the projected algebraic horizontal distance in the

Table 1. Different soil characteristics.

Soil Types	ω_q (rad/s)	ζ_q	v_s(m/s)
Firm	15	0.6	400
Medium	10	0.4	200
Soft	5	0.2	150

The data in Table 1 were gathered from [44–46].

longitudinal direction of propagation of waves, and ν_{app} is the surface apparent wave velocity for long distances away from the epicenter, $v_{app} = v_s$ [42]. The shear wave velocity, v_s, depends on the specifications of the soil profile, and Table 1 illustrates the values [44]. Many papers can be used to extract the incoherence values [42,43,45]. $H_q(\omega)$, $t = k, l$, is the FRF for the acceleration response of the related site at the qth support. $H_q(\omega)$ is defined as:

$$H_q(\omega) = \frac{\omega_q^2 + 2i\,.\,\zeta_q.\omega_t.\omega}{\omega_q^2 - \omega^2 + 2i.\zeta_q.\omega_q.\omega}, \tag{7}$$

where the filter frequency and damping ratio at the qth support are denoted by ω_q and ζ_q, respectively. The calculated values of ω_q and ζ_q are listed in Table 1.

As mentioned above, the simulation process of earthquake ground motion considering spatial variation is different from standard methods used for generating acceleration time histories. In other words, to simulate a traveling wave, a Power Spectral Density Function (PSDF), a response spectrum, and a coherence function must be considered. The time series are randomly generated using defined PSDF and fitted to a predefined response spectrum, while the coherency function relates the simulated series at different simulation points. Therefore, it seems logical that by getting away from the first simulation location, the similarity of simulated series is reduced and at a length of about 500 meters from the first simulation point, the simulated record has the slightest resemblance to the primary record. There are two methods developed for simulating the ground motions. The unconditional method uses a PSDF, a response spectrum, and a coherence function,while the conditional method utilizes a power spectral density function derived from a real earthquake event, a response spectrum, and a predefined coherence function. The time series generated by the unconditional method does not include the inherent characteristics of a specific record, showing less tendency to diverge. In addition, the simulated time series by the conditional method contains the features of the original record while having the highest tendency to diverge. To better understand the simulation process of seismic ground motions, it is recommended to refer to Ref. [40].

4. Numerical study and bridges descriptions

For a numerical study, a reinforced concrete curved plan bridge was chosen from a prototype portfolio prepared by PEER Center. The bridge has a box-girder deck and single-column bent designed for California seismic exposure [47]. As mentioned before, the dynamic properties of the structure have a direct effect on the responses. Thus, to make a variety in terms of mass and stiffness, two other bridges are derived from elongating and shortening of the main structure. Also, to change the lateral stiffness, three different column heights were considered. Table 2 represents the specifications of various considered bridges. Bridge Type B with column height of $H2$ is the main bridge and it corresponds to the Bridge Type 1 in [47]. The Caltrans SDC (2006) requirements are used in the properties of column sections to prevent shear failure [48]. The connections between columns and the deck are rigid. The AASHTO (2004) guidelines defined the minimum bridge radius regarding the design roadway speed and

Table 2. Specifications of the bridge types.

Radios/ column height	Type A $R = 152$ (m)	Type B $R = 305$ (m)	Type C $R = 503$ (m)
H1	4.3 (m)	4.3 (m)	4.3 (m)
H2	6.7 (m)	6.7 (m)	6.7 (m)
H3	15.0 (m)	15.0 (m)	15.0 (m)
Span 1	17.1 (m)	36.6 (m)	54.2 (m)
Span 2	23.3 (m)	45.7 (m)	77.1 (m)
Span 3	24.2 (m)	45.7 (m)	80.1 (m)
Span 4	23.3 (m)	45.7 (m)	77.1 (m)
Span 5	17.1 (m)	36.6 (m)	54.2 (m)
D	1.52 (m)	1.22 (m)	1.22 (m)

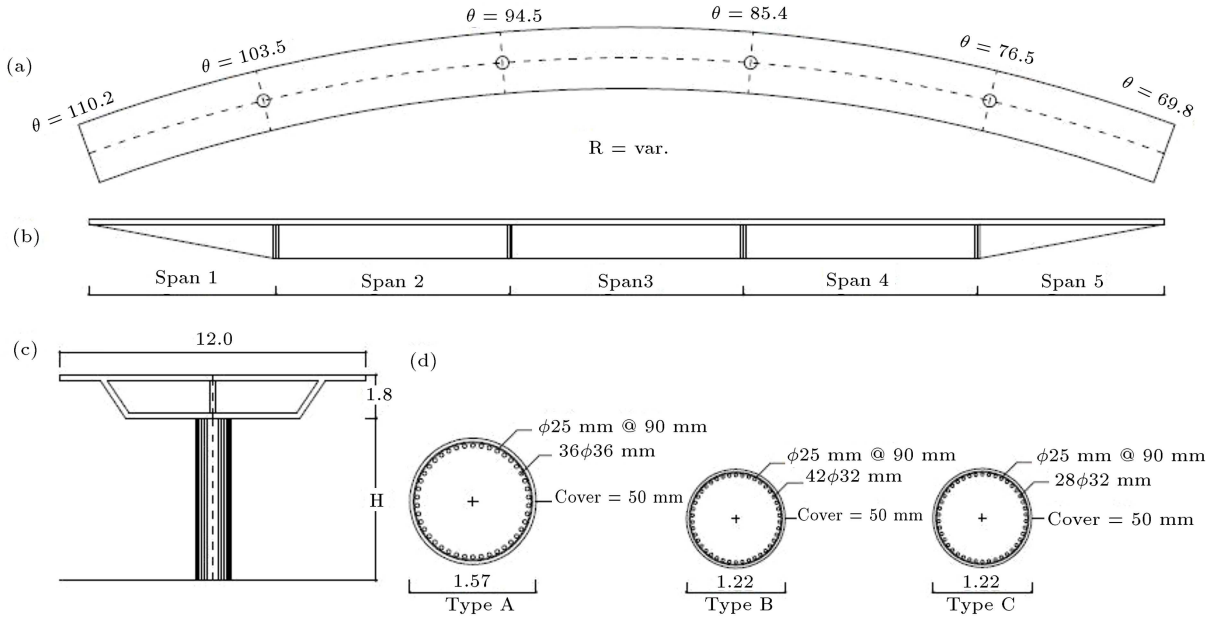

Figure 1. Geometric properties of the bridges.

Table 3. The deck properties.

Area	A	5.72 m^2
Compressive strength	$f'_{c.\ deck}$	34.47 MPa
Elasticity modulus	E	27596 MPa
Shear modulus	G	11498 MPa
Moment of inertia about y-axis	I_z	2.81 m^4
Moment of inertia about z-axis	I_y	53.87 m^4
Torsional moment of inertia	J_t	6.03 m^4
Prestressing force	F_p	31136 kN

Table 4. The characteristics of concrete and steel.

Confined concrete		
Compressive strength	f'_{cc}	46.63 MPa
Strain at f'_{cc}	ε_{cc}	0.0089
Crushing strength	f_{cu}	38.72 MPa
Crushing strain	ε_{cu}	0.0365
Elasticity modulus	E_c	24692 MPa
Tensile strength	f_t	2.76 MPa
Unconfined concrete		
Compressive strength	f'_{co}	27.6 MPa
Strain at f'_{co}	ε_{psco}	0.002
Crushing strength	f_{pcu}	0.0 MPa
Sapling strain	ε_{sp}	0.005
Steel		
Yield strength	f_{ye}	470 MPa
Elasticity modulus	E_s	200000 MPa

the super-elevation rate. Nine bridges with three different radii and column heights are studied. Figure 1 illustrates the geometric properties of the bridges. The Finite Element Models (FEMs) are developed by the OpenSees framework [38]. A schematic view of the finite element models is illustrated in Figure 2. The first simulation point is located at the left abutment, the next ones from columns 1 to 4, and the last point located at the right abutment. In the FEM, the deck is modeled using the Elastic-Beam-Column element (EBC) and is assumed to be elastic. The characteristics of the deck are gathered in Table 3. To obtain accurate results, the deck is divided into 40 segments, and such discretization makes the uniform distribution of mass necessary for computing the corresponding mode shapes. The Fiber-section Beam-Column (FBC) element is used to model the columns [48]. Each column is divided into four segments that are connected to the deck by a rigid element and fixed on the top of the foundation. The longitudinal reinforcement of columns is modeled using the Steel02 material of the Giuffre-Menegotto-Piano model with isotropic strain hardening (Manual of the OpenSees, 2009). To model the behavior of the confined and unconfined concretes, the stress-strain relationship is used, as suggested by Caltrans SDC [49]. The OpenSees defined materials including Concrete01, Concrete02, and Steel02 used for unconfined concrete, confined concrete, and rebar, respectively. The specifications of the used materials are gathered in Table 4.

The moment and shear specifications of columns are presented in Table 5. From the calculated shear

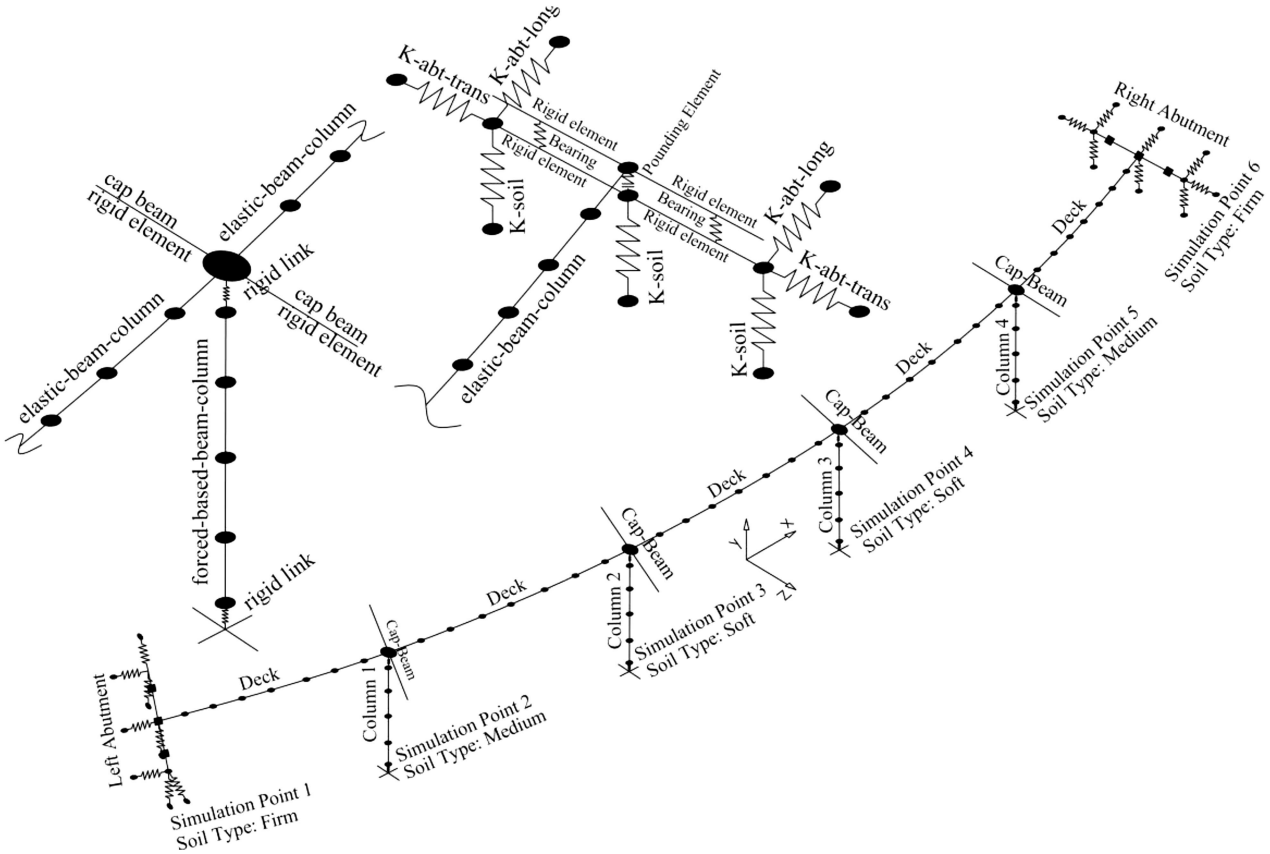

Figure 2. Simplified demonstration of the finite element models.

Table 5. Moment and shear capacities of columns.

Yield curvature, φ_y (rad/m)	0.003976
Yield moment, M_y (kNm)	6650
Plastic moment, M_p (kNm)	8985
Nominal shear strength, V_n (kN)	6278
$M_p/V_n\, d$	1.17
Shear span to depth ratio longitudinal, $H_{col}/2d$	2.75

capacities, it is clear that the columns are safe from shear failure. The non-linear zero-length elements are used to model the abutments based on the information presented in Table 6. In the vertical and transverse directions, the stiffness of the soil is computed and assigned to elastic zero length elastic elements. To avoid pounding, a compression gap of 0.10 m (4 in) is defined to consider the expansion joint. The transverse response of the abutment is represented by an EPP force-deformation response backbone curve proposed by Caltrans SDC. The stiffness of the soil under the embankment was estimated by Zhang and Makris (2002) in the vertical direction and assigned to elastic zero-length elements [50]. The dynamic properties of the analyzed bridges are listed in Table 7. In this study, it is assumed that the abutments are situated on the firm soil to include the site-response effects. Thus, columns 1 and 4 are situated on the medium soil, and columns 2 and 3 are located on the soft soil. Usually, for ordinary bridges, the first two mode shapes are coupled

Table 6. Geometrical and mechanical characteristics of the abutments.

Back wall (with reinforced concrete wall connected to the abutments)	8.23 m
Wing wall (with reinforced concrete wall connected to the abutments)	3.96 m
$K_{abt}\, long$	101811 kN/m
$P_{bw}\, long$	3860 kN
$K_{abt}\, trans$	243753 kN/m
$P_{bw}\, trans$	1,656 kN
ρ	1760 kg/m^3
υ_s	150 m/s
E_{soil}	110972 MPa

Table 7. Dynamic characteristics of the analyzed bridges.

Type/column height	$H1 = 4.3$ (m)		$H2 = 6.7$ (m)		$H3 = 15.0$ (m)	
	Current study	**Tondini and Stojadinovic**	**Current study**	**Tondini and Stojadinovic**	**Current study**	**Tondini and Stojadinovic**
$R1 = 152.0$ (m)	$T1 = 0.280$ (s) $T2 = 0.280$ (s) $T3 = 0.200$ (s)	$T1 = 0.285$ (s) $T2 = 0.285$ (s) $T3 = 0.206$ (s)	$T1 = 0.540$ (s) $T2 = 0.540$ (s) $T3 = 0.480$ (s)	$T1 = 0.560$ (s) $T2 = 0.550$ (s) $T3 = 0.495$ (s)	T1=1.530 (s) $T2 = 1.470$ (s) $T3 = 1.280$ (s)	$T1 = 1.550$ (s) $T2 = 1.501$ (s) $T3 = 1.294$ (s)
$R2 = 305.0$ (m)	$T1 = 0.860$ (s) $T2 = 0.850$ (s) $T3 = 0.480$ (s)	$T1 = 0.870$ (s) $T2 = 0.855$ (s) $T3 = 0.485$ (s)	$T1 = 1.000$ (s) $T2 = 1.000$ (s) $T3 = 0.780$ (s)	$T1 = 1.073$ (s) $T2 = 1.042$ (s) $T3 = 0.765$ (s)	$T1 = 2.260$ (s) $T2 = 2.050$ (s) $T3 = 2.000$ (s)	$T1 = 2.290$ (s) $T2 = 2.120$ (s) $T3 = 2.067$ (s)
$R3 = 503.0$ (m)	$T1 = 1.750$ (s) $T2 = 1.720$ (s) $T3 = 1.190$ (s)	$T1 = 1.770$ (s) $T2 = 1.740$ (s) $T3 = 1.210$ (s)	$T1 = 1.820$ (s) $T2 = 1.790$ (s) $T3 = 1.350$ (s)	$T1 = 1.843$ (s) $T2 = 1.804$ (s) $T3 = 1.363$ (s)	$T1 = 3.120$ (s) $T2 = 2.760$ (s) $T3 = 2.400$ (s)	$T1 = 3.250$ (s) $T2 = 2.820$ (s) $T3 = 2.483$ (s)

Table 8. The characteristics of the main time series.

Event	Year	M	R (km)	PGA (major)	Station	Soil	Mechanism
Chi-Chi	1999	7.6	6.8	0.350	Chiayi	Soft soil	Reverse-oblique
Kobe	1995	6.9	22.5	0.380	Kakogawa	Medium soil	Strike-slip
Kobe	1995	6.9	95.7	0.135	HIK	Medium soil	Strike-slip
Kocaeli	1999	7.4	91.3	0.180	Fatih-Tomb	Soft soil	Strike-slip
Landers	1992	7.5	44.4	0.123	Barstow	Soft soil	Reverse-oblique
Loma Prieta	1989	7.1	13.9	0.230	Hollister	Soft soil	Reverse-oblique
Northridge	1994	6.8	9.5	0.54	Arleta	Soft soil	Reverse
Northridge	1994	6.8	23.8	0.31	Malibu	Soft soil	Reverse
San Fernando	1971	6.6	23.7	0.17	Pasadana	Medium soil	Reverse
San Fernando	1971	6.6	79.8	0.094	Santa Anita	Soft soil	Reverse

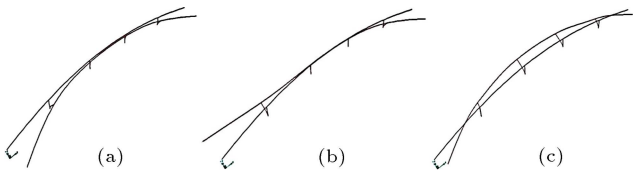

Figure 3. The first three modes (a), (b), and (c), respectively, of the analyzed bridges regarding Table 7.

with the transverse and longitudinal mode shapes. The mode shapes are illustrated in Figure 3. In Table 6, the back wall and wing wall are reinforced concrete walls that are connected to the abutments. The back walls are situated in the direction perpendicular to the longitudinal axis of the bridge and the wing walls are located parallel to the longitudinal axis of the bridge.

5. Input ground motions

In this study, the existing (known) earthquakes were selected from the Pacific Earthquake Engineering Research Center (PEER) Strong Motion Database [51]. The Peak Ground Accelerations (PGA) of the records vary from 0.11 to 0.54 (g) and consist of low and high moment magnitudes and large and small epicentral distances. These records are then used to simulate the correlated ground motions at simulation points in Figure 2. For each ground motion, ten series of simulated records were generated and a total of a hundred correlated ground motions were imposed on each bridge. The Incremental Dynamic Analysis (IDA) is used to evaluate the non-linear behavior of the bridges. Based on the conditional simulation technique described before, a Matlab code is developed and the required time series are generated. To ensure the accuracy of the process, the Power Spectral Density (PSD) of generated records is compared with the original time history. Figure 4 illustrates a sample of simulated records (original record: Northridge) and the corresponding PSDs. It is clear from Figure 4(m) and (n) that the simulated records are in good agreement with the original record. Also, due to the soil type defined for the simulation points, the corresponding response spectra are different. The maximum acceleration and velocity response were calculated for stations 3 and 4 situated on the soft soils. The simulated time series imposed on supports in X, Y, and Z directions. The characteristics of the primary time series are illustrated in Table 8.

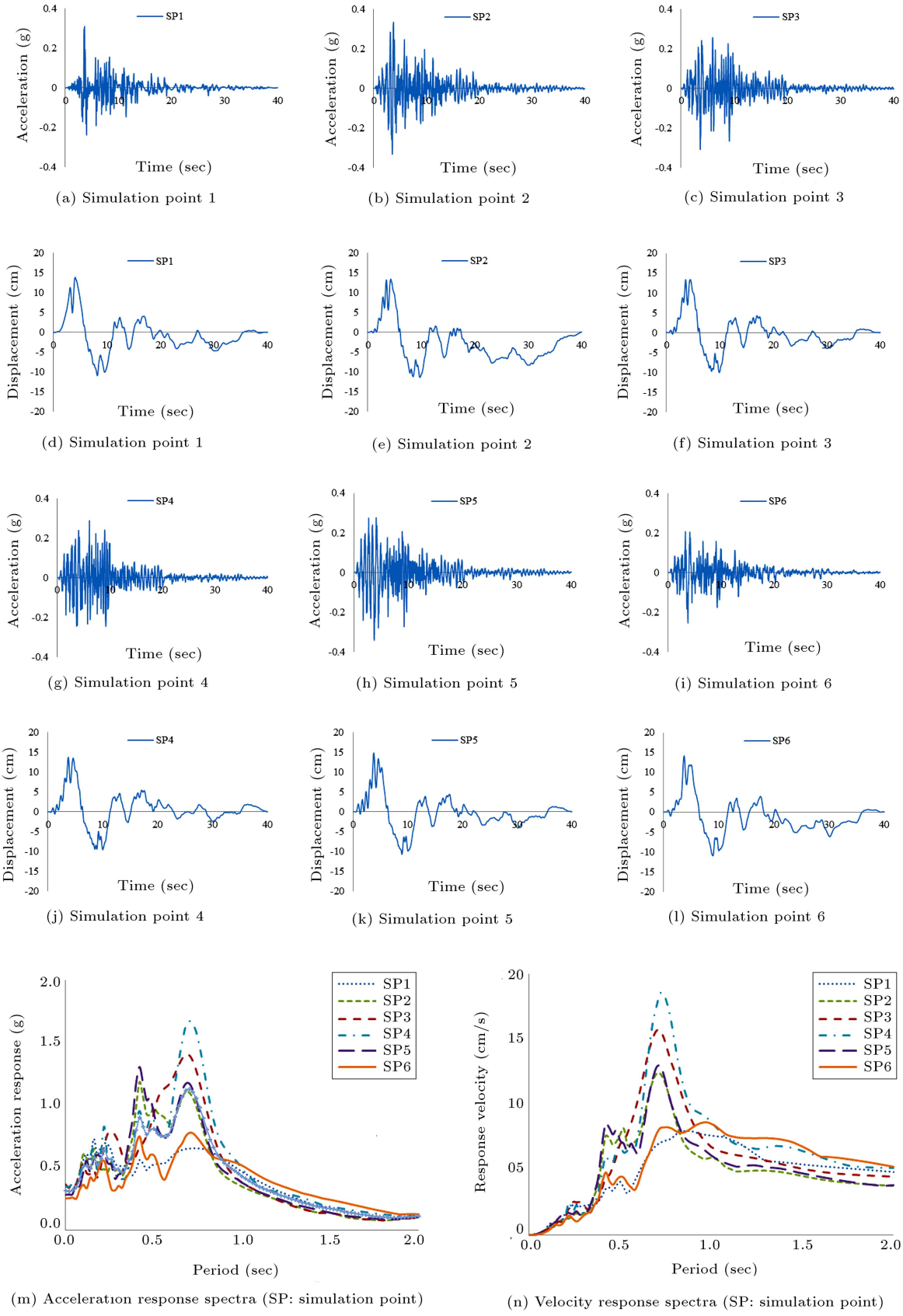

(a) Simulation point 1 (b) Simulation point 2 (c) Simulation point 3

(d) Simulation point 1 (e) Simulation point 2 (f) Simulation point 3

(g) Simulation point 4 (h) Simulation point 5 (i) Simulation point 6

(j) Simulation point 4 (k) Simulation point 5 (l) Simulation point 6

(m) Acceleration response spectra (SP: simulation point)

(n) Velocity response spectra (SP: simulation point)

Figure 4. Simulated acceleration and displacement time history and corresponding response spectrums for Northridge earthquake.

Table 9. Performance levels related to damage states and drift limits [52].

Performance level	Damage state	Drift
Fully operational, immediate occupancy	No damage	$< 0.2\%$
Operational, damage control, moderate	Repairable	$< 0.5\%$
Life safe-damage state	Irreparable	$< 1.5\%$
Near collapse, limited safety	Severe	$< 2.5\%$
Collapse		$> 2.5\%$

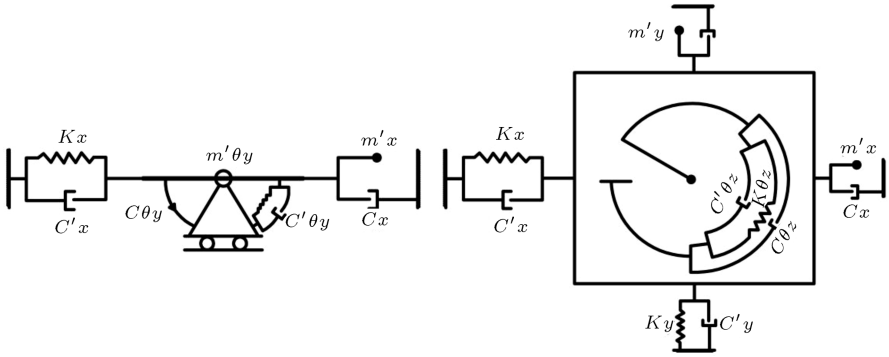

Figure 5. Springs, masses, and dashpots layout.

6. Demand and limit-state model, load, and soil combinations

Usually, the results of a set of Non-linear Time-History Analyses (NTHAs) are used for relating the IMs to seismic demand (D, peak responses) by a linear or non-linear regression in a log-normal space. In the current study, the IMs are defined as peak ground acceleration extensively used for risk assessment of bridges by many researchers. For the assumed bridges described in Table 2, the non-linear time history analysis is performed using 100 pairs of displacement time history at six locations illustrated in Figure 2. For each analysis, the drift ratio of the columns was recorded in longitudinal and transverse directions. Then, based on the recorded response outputs (demand) and corresponding PGA, the demand model is formed by regression in a log-normal space. As mentioned in Eq. (1), to form fragility curves, a capacity-based limit state model is necessary to evaluate the damage to the structure. The performance levels corresponding to damage states and drift limits are presented in Table 9 [52]. To carry out a comprehensive probabilistic evaluation of the bridges defined in Table 2, a set of non-linear uniform and non-uniform seismic excitations is performed with and without considering the Soil-Structure Interaction (SSI) effects. Finally, the fragility curves are calculated accordingly. Previous studies found that the rotational responses were induced by SSI effects. The dynamic response of super structures obtained on rigid foundations may be increased or decreased due to the impact of soil-structure interactions. In the current study, a simplified model that consists of some springs, masses, and dashpots is used to study the SSI effects on the dynamic response of the structure (Figure 5). The required information is considered based on Table 1 and the soil density defined as $\rho = 1800$ N/m^3. Table 10 presents all data used to model the soil-structure interaction [53].

As mentioned, soil conditions vary at different simulation points; in addition, four different loading combinations are defined including uniform and non-uniform excitations with and without consideration of SSI effects.

7. Incremental Dynamic Analysis (IDA), demand model

Incremental Dynamic Analysis (IDA) is an efficient method to estimate structural performance under several seismic records [54]. IDA results are used to produce the fragility curves that describe the damage measure versus intensity measure. The seismic records can be real or synthetic and are generated artificially. As mentioned before in this study, some real records are selected and simulated to generate correlated ground motions and consequently, the generated records contain the specifications of the real (original) records such as amplitude, frequency, duration, energy content, number of cycles, and phase. In the IDA method,

Table 10. Data used to model SSI effects [53].

Motion	Horizontal	Vertical		Rocking		Torsional
Equivalent radius, r_0	$\sqrt{\frac{A_0}{\pi}}$	$\sqrt{\frac{A_0}{\pi}}$		$\sqrt[4]{\frac{4I_0}{\pi}}$		$\sqrt[4]{\frac{2I_0}{\pi}}$
Aspect ratio, $\frac{z_0}{r_0}$	$\frac{\pi}{8}(2-\vartheta)$	$\frac{\pi}{4}(1-\vartheta)\left(\frac{c}{c_s}\right)^2$		$\frac{9\pi}{32}(1-\vartheta)\left(\frac{c}{c_s}\right)^2$		$\frac{9\pi}{32}$
Poisson's ratio, υ	All ϑ	$\leq \frac{1}{3}$	$\frac{1}{3} < \vartheta < \frac{1}{2}$	$\leq \frac{1}{3}$	$\frac{1}{3} < \vartheta \leq \frac{1}{2}$	All ϑ
Wave velocity, c	c_s	c_p	$2c_s$	c_p	$2c_s$	c_s
Trapped mass, ΔM ΔM_θ	0	0	$2.4\left(\vartheta-\frac{1}{3}\right)\rho A_0 r_0$	0	$1.2\left(\vartheta-\frac{1}{3}\right)\rho I_0 r_0$	0
Discrete element model	$K=\rho c^2 A_0/z_0$ $C=\rho c A_0$			$K_\theta=3\rho c^2 I_0/z_0$ $C_\theta=\rho c I_0$ $M_\theta=\rho I_0 z_0$		

Note: A_0 is area of the mat; I_0 moment of inertia; ϑ Poisson's ratio; ρ mass density; c_s shear-wave velocity; and c_p dilatational-wave velocity.

the nonlinear dynamic analysis is performed by a stepwise increase of seismic intensity (PGA) until the structure reaches predefined instability. In this study, the columns drift ratio is chosen as an efficient indicator, and the corresponding performance levels and related damage limit states are presented in Table 9 [52]. To develop the fragility curves, each bridge was analyzed in 100 simulated records: 20 times for each record were attempted at different PGA levels that varied from 0.1 g to 2.0 g and a total of 9000 NTHAs were performed. Figures 6, 7, and 8 illustrate the IDA curves for columns 1, 2, 3, and 4 under uniform and non-uniform excitations with and without the SSI effects using ten original records. Comparison of Figures 6, 7, and 8 ((a), (b), (c), and (d)) indicates that under uniform excitations, the behavior of the columns is the same, while the results are different under non-uniform excitations. Moreover, regarding Figures 6, 7, and 8 ((e), (f), (g), and (h)), it is clear that the columns under non-uniform excitations exhibit different behavior compared to the same results under uniform excitations. Despite the form of excitations, the effect of soil condition is visible. To explore the best demand model in the following, the main bridge (type B, R2H2, and Table 2) was selected, and under various load cases, the corresponding demand model was extracted. Figure 9 depicts the demand model of columns 1 and 3 for the bridge under different load combinations. The results confirm that the linear demand model is appropriate and used for developing fragility curves.

8. Developing fragility curves

Based on the results of IDA analysis and the demand models, the fragility curves are developed. Thus, first, the fragility curves due to uniform and non-uniform excitations are compared to each other, and then the effect of SSI is included. For uniform excitations of the bridges, it is assumed that the soil beneath the abutments and columns is the same. For non-uniform excitations, the soil conditions are different, as mentioned before. Figures 10, 11, and 12 compare the Damage Exceedance Probability (DEP) of the columns for bridge types A, B, and C under different performance limit states. As shown in the figures, the bridges for immediate occupancy performance level almost showed the same results under uniform and non-uniform excitations. It means that the behavior of columns is linear and uncracked. The differences between damage probabilities exceeding limit states increase for life safety and collapse prevention limit states. Moreover, it is clear that the probability of failure is a function of bridge length. Based on Figures 10, 11, and 12, it is evident by elongating the bridge, the DEP increases either. For example, the probability of failure is about 50% for bridge types A, B, and C under uniform excitations; accordingly, life safety limit states are 0.45 g, 0.55 g, and 0.9 g, respectively. Furthermore, from the results, the probability of failure for non-uniform excitations increased compared to the uniform excitations. The differences between possibilities of failure for various limit states

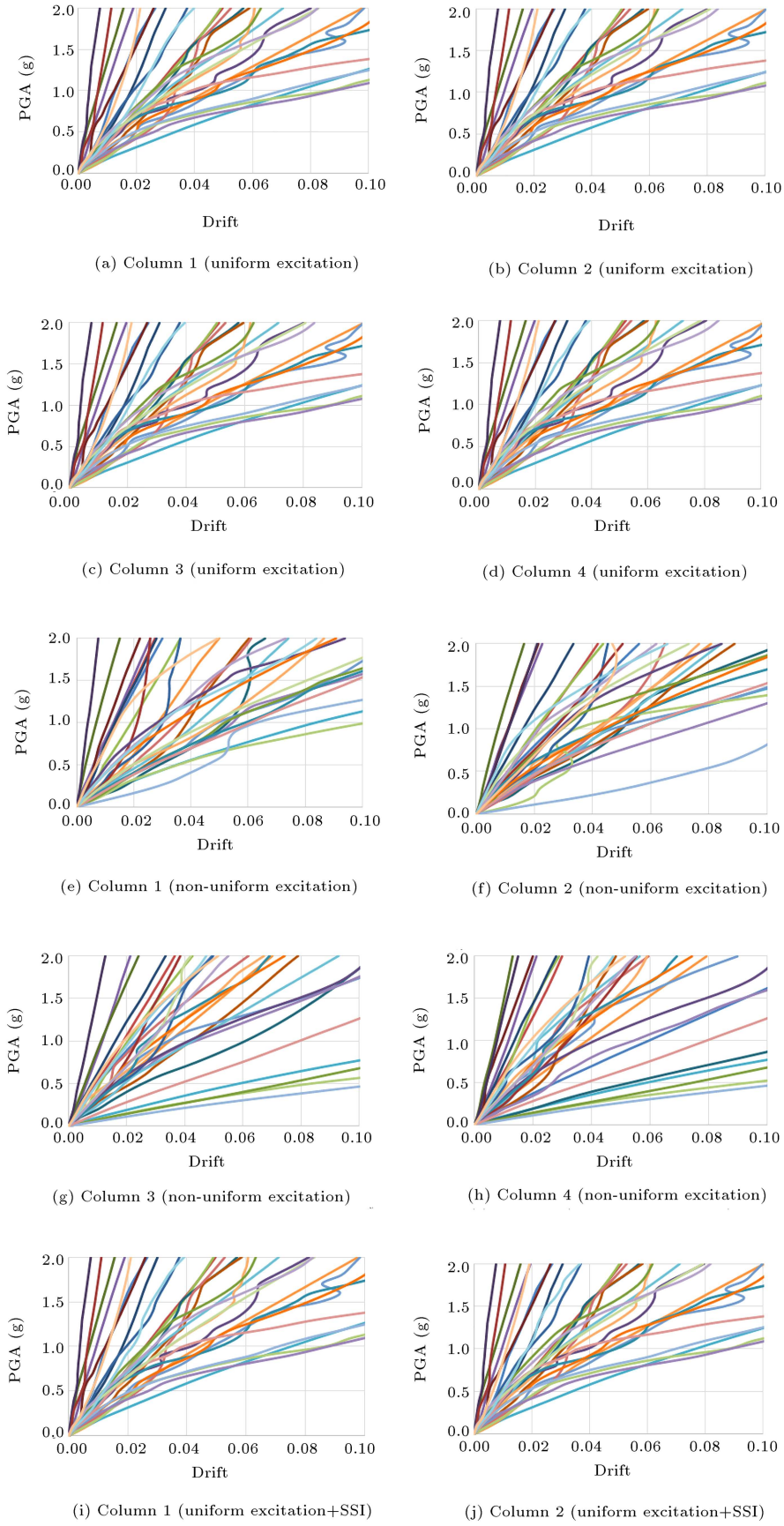

(a) Column 1 (uniform excitation)

(b) Column 2 (uniform excitation)

(c) Column 3 (uniform excitation)

(d) Column 4 (uniform excitation)

(e) Column 1 (non-uniform excitation)

(f) Column 2 (non-uniform excitation)

(g) Column 3 (non-uniform excitation)

(h) Column 4 (non-uniform excitation)

(i) Column 1 (uniform excitation+SSI)

(j) Column 2 (uniform excitation+SSI)

Figure 6. IDA curves for columns 1, 2, 3, and 4 under uniform and non-uniform excitations; bridge type A.

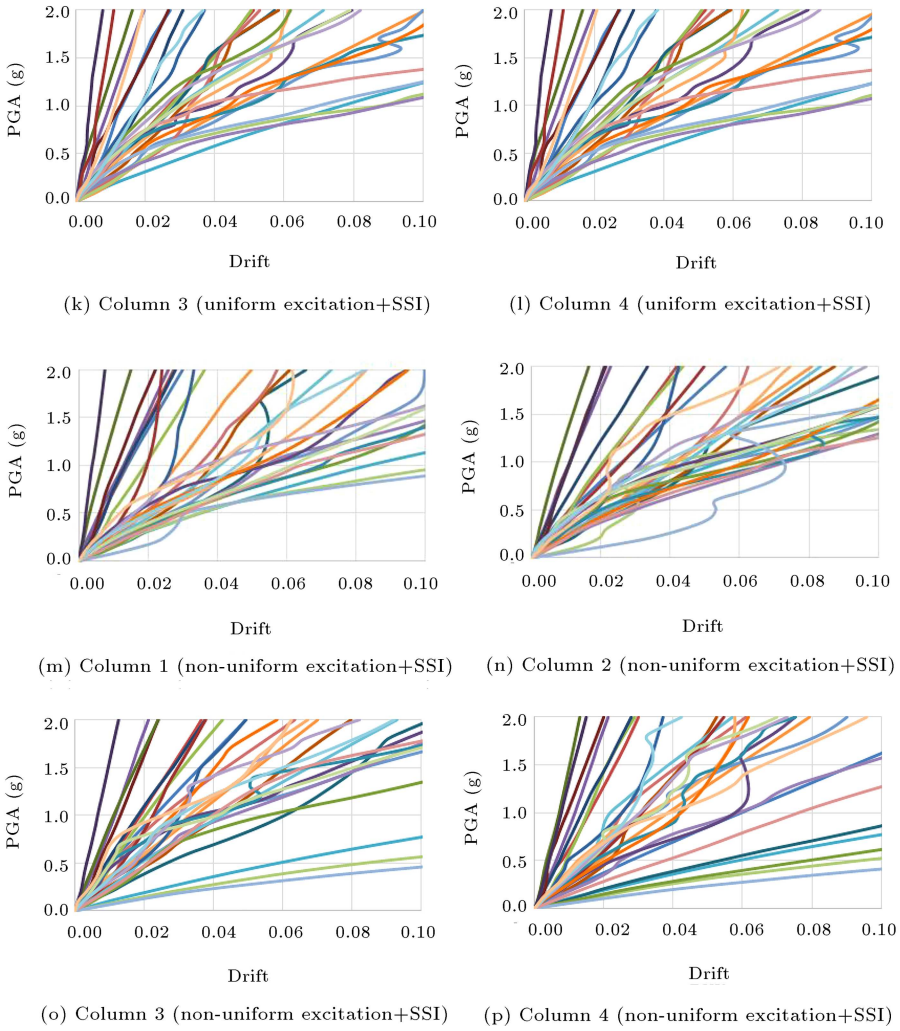

Figure 6. IDA curves for columns 1, 2, 3, and 4 under uniform and non-uniform excitations; bridge type A (continued).

decreased with an increase in the bridge length, while the damage exceedance probability increased. This means that reducing the radius of curvature harms short-span bridges. Also, comparing the results for different columns revealed that the soft soils significantly increased the DEP. For example, considering the DEPs of columns 2 and 3 for collapse prevention limit state, the corresponding PGAs of DEPs about 50% are (1.65, 1.30)-(0.75, 0.60)-(0.60, 0.55) for the columns, respectively. The recorded results for the columns show that the IMs level required for a DEP about 50% was reduced by around 20% for the column situated on the soft soil. Figures 13, 14, 15, and 16 depict the fragility curves of the bridge types A, B, and C (R1H1, R2H2, and R3H3), respectively, under non-uniform excitations, considering soil-structure impact.

Based on the outcomes of the comparison between fragility curves of uniform and non-uniform excitations, the effects of soil-structure interactions included non-uniform NTHAs and fragility curves developed for the bridges types A, B, and C for collapse prevention limit state. The results show that the effects of SSI in short bridges can be neglected, while for long-span bridges, the damage exceedance probability increased due to SSI effects. Regarding the graphs, it is evident that the SSI slightly affected bridge type B, while for the bridge type C, the differences between fragility curves with and without SSI effects are significant. It is implied that for long-span bridges and a soil type defined in this study, a combination of spatially varying ground motions and soil structure effects can increase the responses remarkably.

9. Conclusion

In this study, a fragility assessment of different reinforced concrete bridges was conducted. The effects of incoherence, wave-passage, and soil condition included simulating the correlated arrays using conditional simulation method based on the predefined time histories. The generated time series were converted

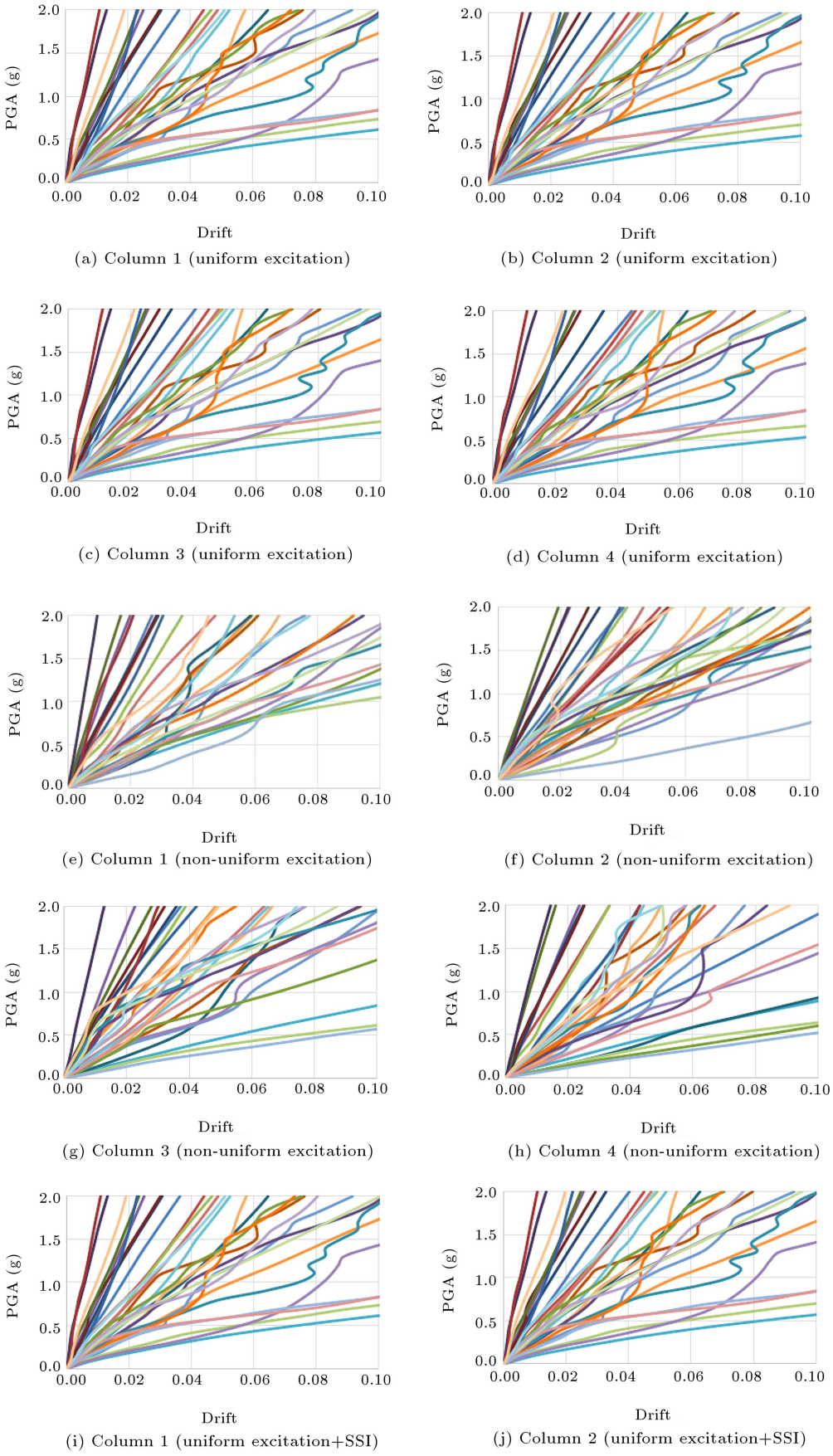

(a) Column 1 (uniform excitation)

(b) Column 2 (uniform excitation)

(c) Column 3 (uniform excitation)

(d) Column 4 (uniform excitation)

(e) Column 1 (non-uniform excitation)

(f) Column 2 (non-uniform excitation)

(g) Column 3 (non-uniform excitation)

(h) Column 4 (non-uniform excitation)

(i) Column 1 (uniform excitation+SSI)

(j) Column 2 (uniform excitation+SSI)

Figure 7. IDA curves for columns 1, 2, 3, and 4 under uniform and non-uniform excitations; bridge type B.

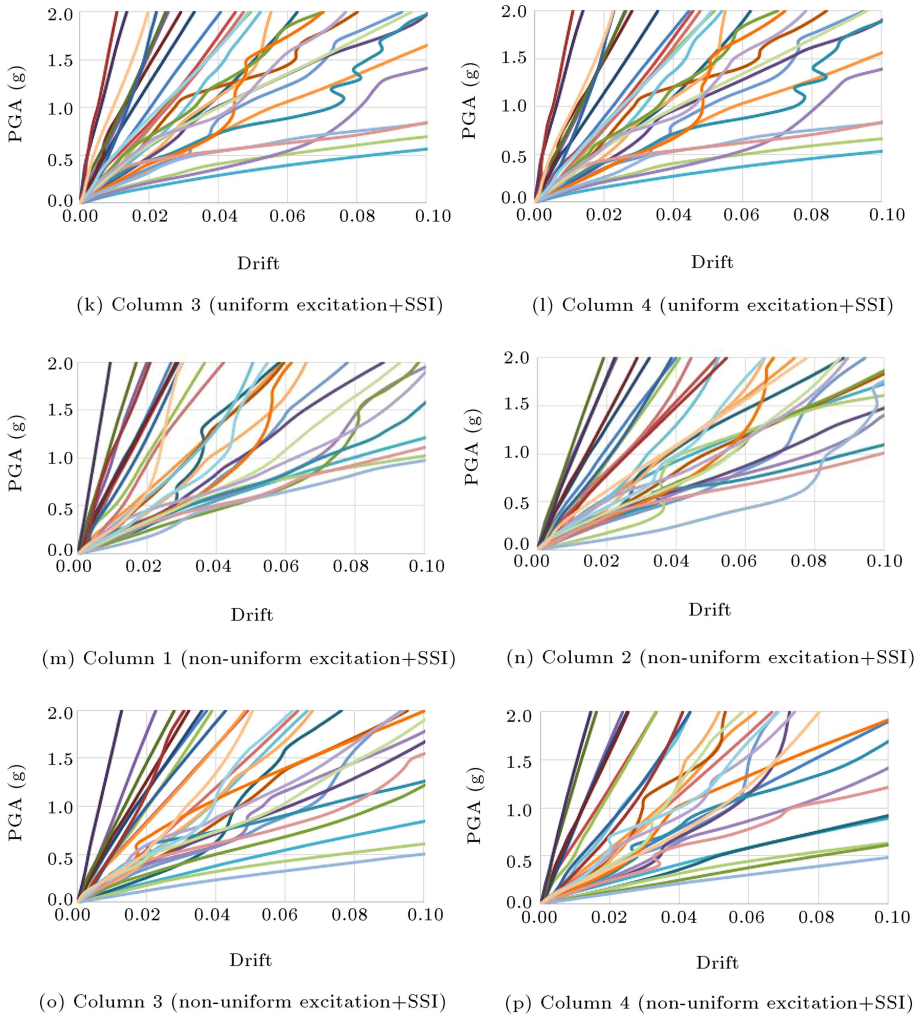

Figure 7. IDA curves for columns 1, 2, 3, and 4 under uniform and non-uniform excitations; bridge type B (continued).

into the corresponding displacement series to perform multiple-support analyses. For the numerical survey, a reinforced concrete bridge from the Caltrans bridge portfolio, which was designed and constructed in California, was selected and two other bridges were derived from shortening and elongating the main bridge. Moreover, to change the stiffness, three different column heights were defined. Totally nine various bridges were studied. To develop the fragility curves, the incremental dynamic analysis was used. Each bridge was analyzed for 20 steps of intensity measure and the process was repeated for ten arrays. In addition, a total of 100 calculations per bridge were carried out. From the results, the linear demand model was produced by linear regression. The fragility curves were developed based on the outcome of uniform and non-uniform excitations. The effect of soil-structure interactions included evaluating the exact results. According to the study, the following conclusions can be extracted:

1. Due to the linear behavior of the bridges, the fragility curves developed for the immediate occupancy limit state on all bridges showed almost the same results. It is clear that the span length adversely affects the probability of failure. In this way, by increasing the span length, the possibility of exceedance to I.O. level occurs at a lower PGA level. Comparison of Figure 10(c) and Figure 12(c) indicates that the PGA level needs to reach the I.O. level reduced from 0.5 g to 0.25 g for a bridge with 152- and 503-meter lengths, respectively;

2. The results illustrate that the probability of failure of the bridges under non-uniform excitation, including the effects of wave passage, incoherency, and soil conditions, is higher than the same results due to uniform excitation;

3. The developed fragility curves show that the variation in soil condition for multiple support structures from stiff to medium or soft remarkably increases the damage exceedance probability. The main

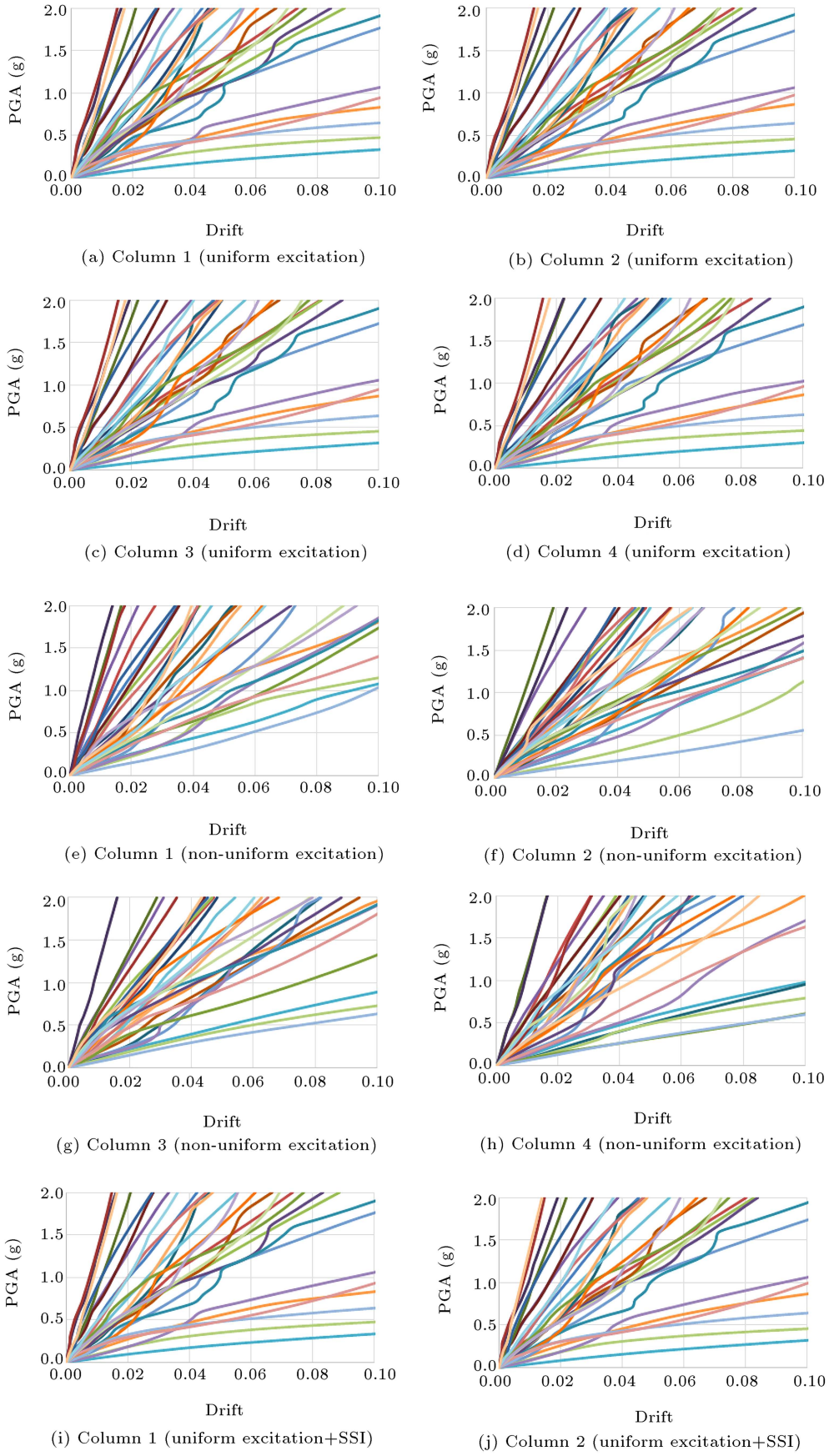

(a) Column 1 (uniform excitation)

(b) Column 2 (uniform excitation)

(c) Column 3 (uniform excitation)

(d) Column 4 (uniform excitation)

(e) Column 1 (non-uniform excitation)

(f) Column 2 (non-uniform excitation)

(g) Column 3 (non-uniform excitation)

(h) Column 4 (non-uniform excitation)

(i) Column 1 (uniform excitation+SSI)

(j) Column 2 (uniform excitation+SSI)

Figure 8. IDA curves for columns 1, 2, 3, and 4 under uniform and non-uniform excitations; bridge type C.

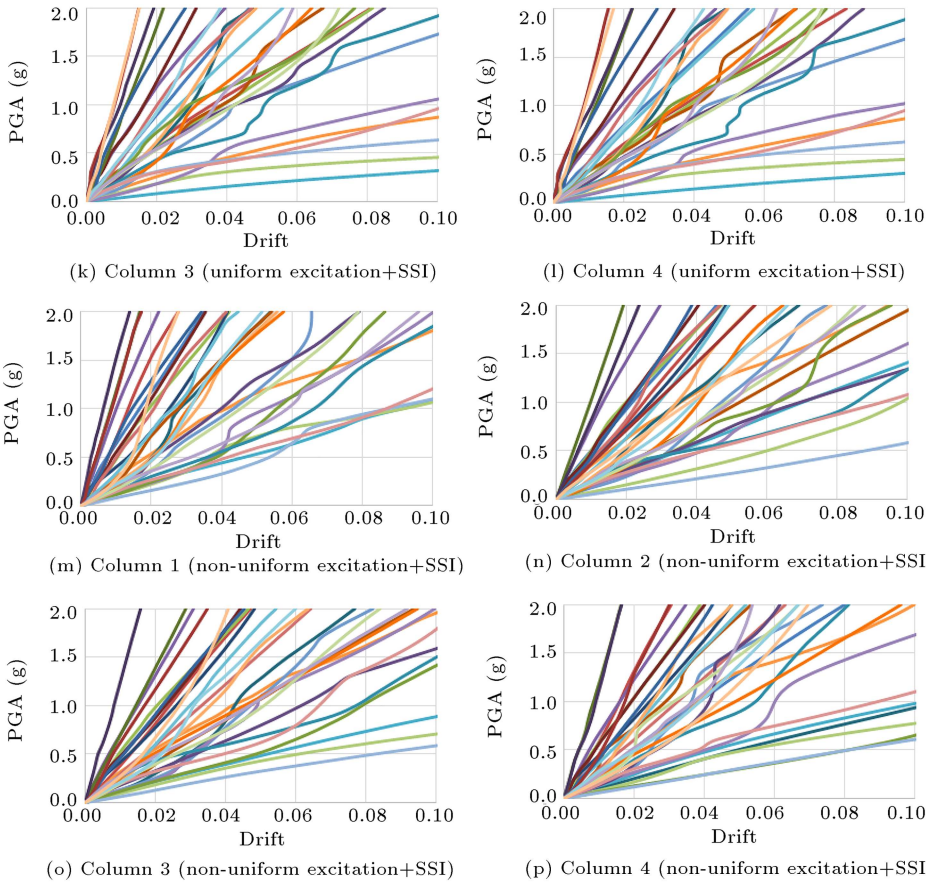

(k) Column 3 (uniform excitation+SSI)
(l) Column 4 (uniform excitation+SSI)
(m) Column 1 (non-uniform excitation+SSI)
(n) Column 2 (non-uniform excitation+SSI
(o) Column 3 (non-uniform excitation+SSI)
(p) Column 4 (non-uniform excitation+SSI

Figure 8. IDA curves for columns 1, 2, 3, and 4 under uniform and non-uniform excitations; bridge type C (continued).

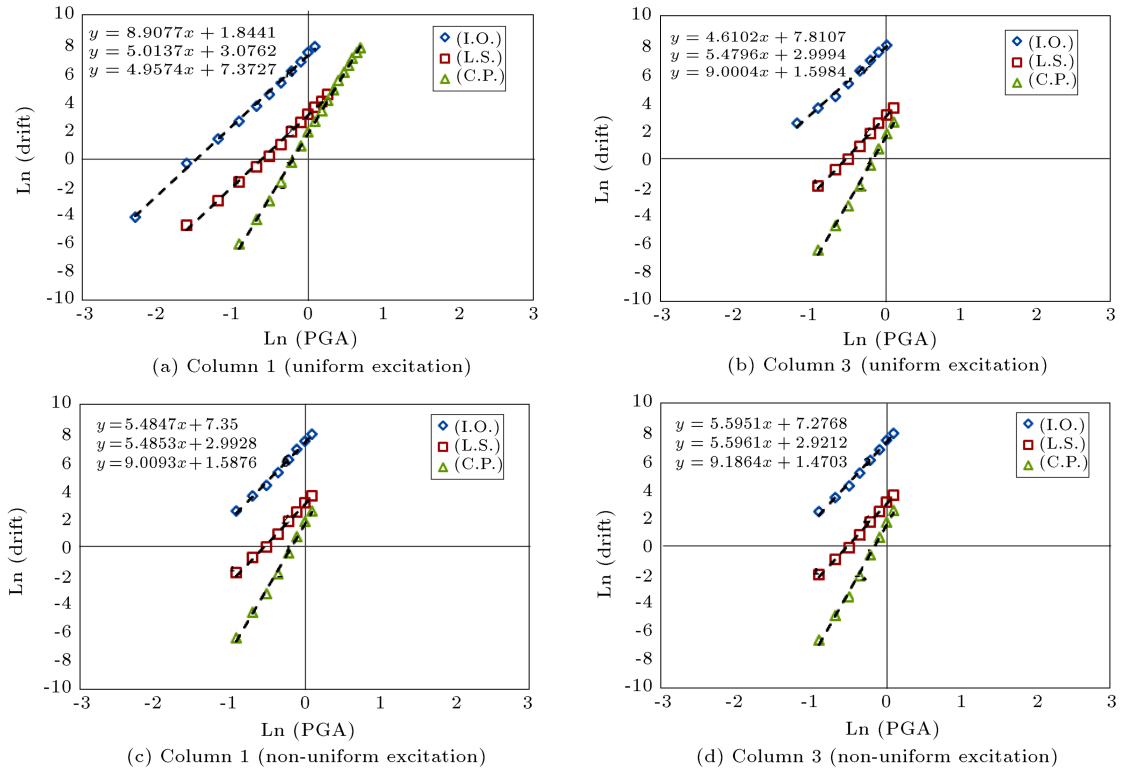

(a) Column 1 (uniform excitation)
(b) Column 3 (uniform excitation)
(c) Column 1 (non-uniform excitation)
(d) Column 3 (non-uniform excitation)

Figure 9. Linear fit demand model for columns 1 and 3; bridge type B.

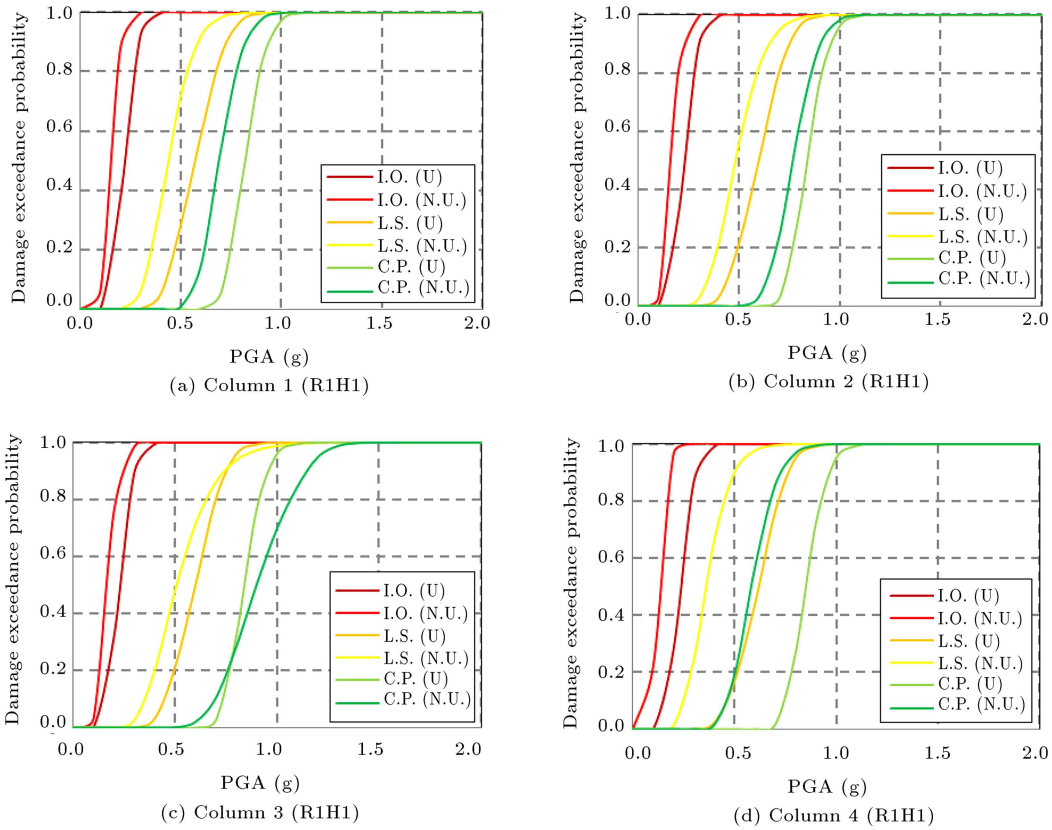

Figure 10. Comparison of damage exceedance probability for the columns of bridge type A (R1H1); I.O. (Immediate Occupancy), L.S. (Life Safety), C.P. (Collapse Prevention), U. (Uniform) and N.U. (Non-Uniform).

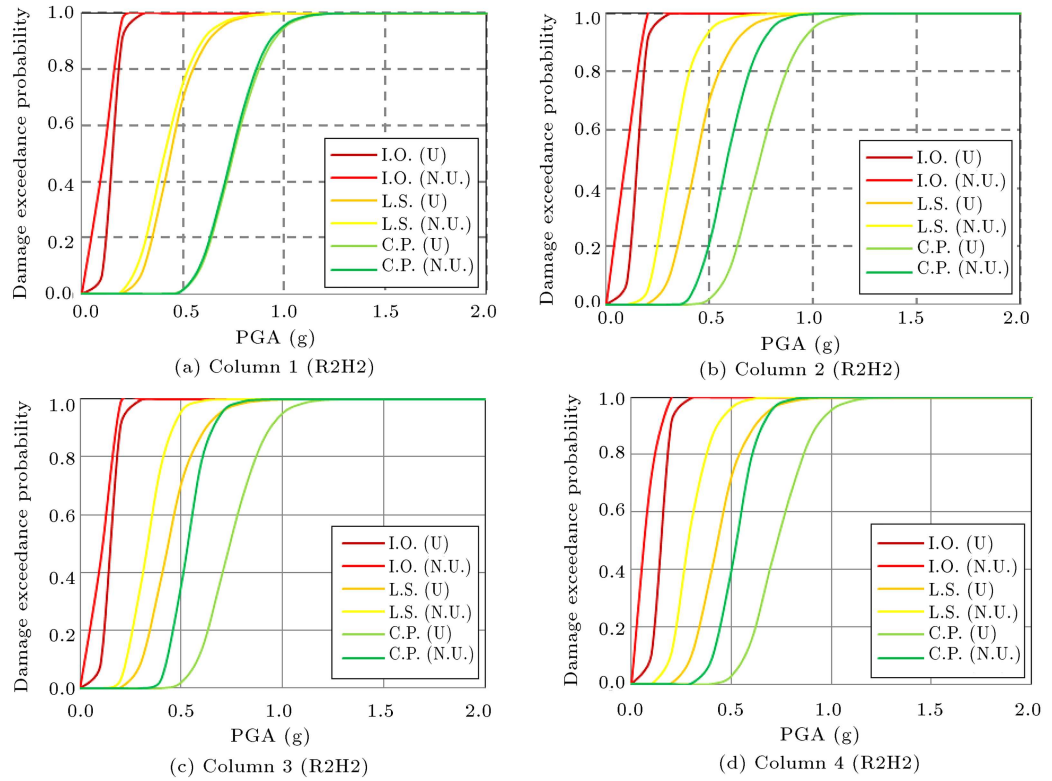

Figure 11. Comparison of damage exceedance probability for the columns of bridge type B (R2H2); I.O. (Immediate Occupancy), L.S. (Life Safety), C.P. (Collapse Prevention), U. (Uniform) and N.U. (Non-Uniform).

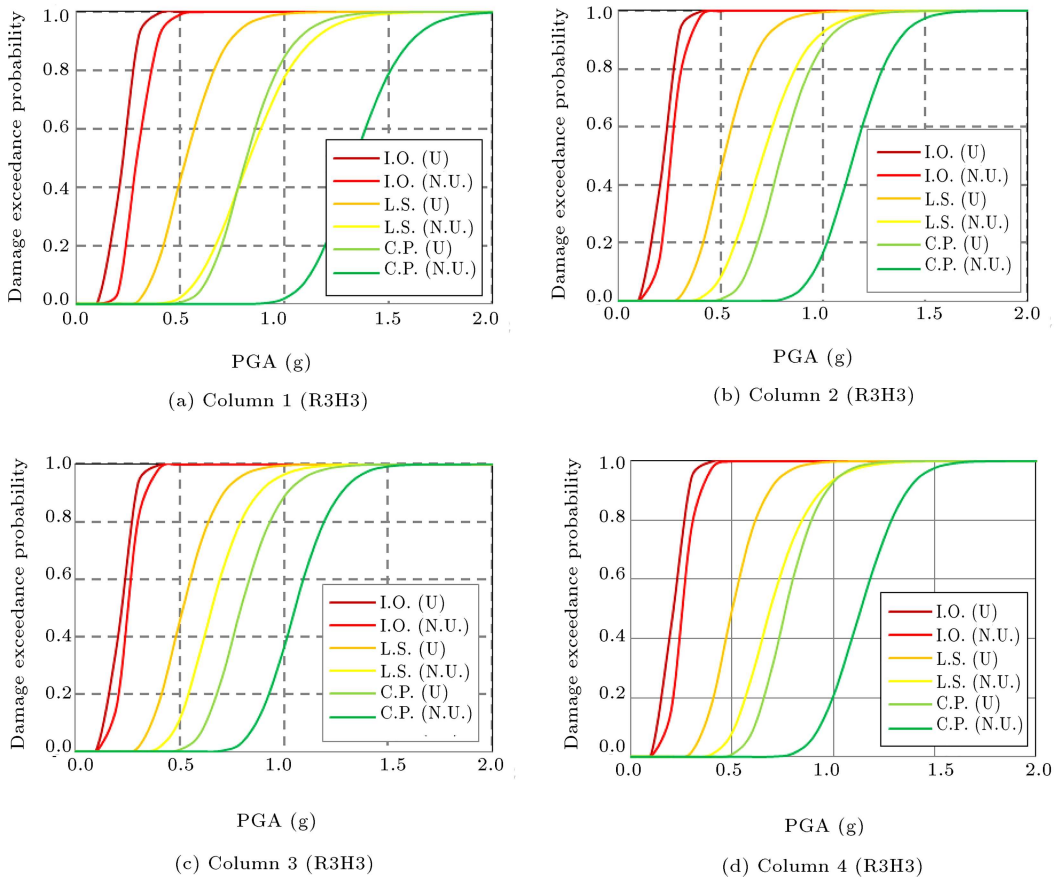

(a) Column 1 (R3H3)

(b) Column 2 (R3H3)

(c) Column 3 (R3H3)

(d) Column 4 (R3H3)

Figure 12. Comparison of damage exceedance probability of columns for bridge type C (R3H3); I.O. (Immediate Occupancy), L.S. (Life Safety), C.P. (Collapse Prevention), U. (Uniform) and N.U. (Non-Uniform).

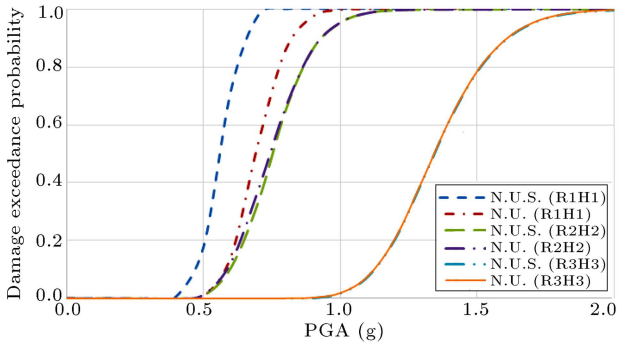

Figure 13. Comparison of damage exceedance probability of the first column for bridge types, A, B and C for Collapse Prevention (C.P.) limit state considering SSI (N.U.: Non-Uniform, N.U.S.: Non-Uniform+SSI).

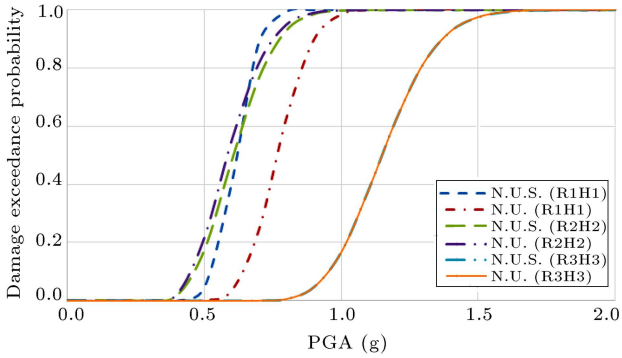

Figure 14. Comparison of damage exceedance probability of the second column for bridge types, A, B and C for Collapse Prevention (C.P.) limit state considering SSI (N.U.: Non-Uniform, N.U.S.: Non-Uniform+SSI).

reason is the local-site effects that increased the dynamic and pseudo-static responses simultaneously;

4. The fragility curves developed regarding the soil-structure interactions demonstrate that in short-span bridges, the effect of SSI is insignificant and can be neglected. In contrast, for long-span bridges, the mentioned effect is noticeable. From Figure 16, it is apparent that for the longest bridge under non-uniform excitations considering SSI effects at PGA level 0.4 g, the damage exceedance probability is five times greater than the same results without SSI effects;

5. Based on the results, considering spatially varying ground motion parameters combined with soil-structure interactions on a varying soil condition significantly increases the damage exceedance probability.

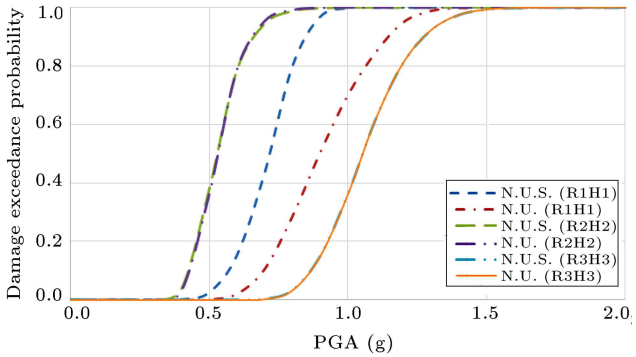

Figure 15. Comparison of damage exceedance probability of the third column for bridge types, A, B and C for Collapse Prevention (C.P.) limit state considering SSI (N.U.: Non-Uniform, N.U.S.: Non-Uniform+SSI).

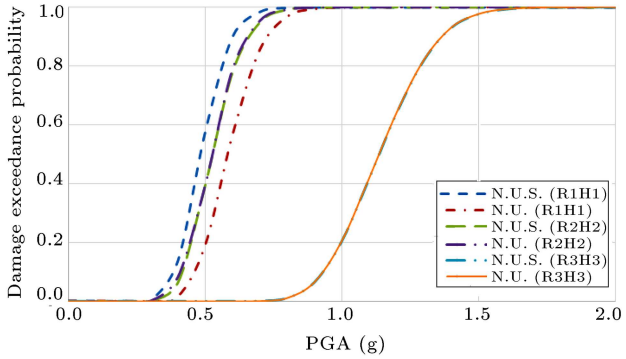

Figure 16. Comparison of damage exceedance probability of the fourth column for bridge types A, B, and C for Collapse Prevention (C.P.) limit state considering SSI (N.U.: Non-Uniform, N.U.S.: Non-Uniform+SSI).

References

1. Zhong, J., Jeon J.S., Yuan, W., et al. "Impact of spatial variability parameters on seismic fragilities of a cable-stayed bridge subjected to differential support motions", *Journal of Bridge Engineering*, **22**(6) (2017).
2. Zhang, J. and Huo, Y.L. "Evaluating effectiveness and optimum design of isolation devices for highway bridges using the fragility function method", *Engineering Structures*, **31**(8), pp. 1648–1660 (2009).
3. Cornell, C.A., Jalayer, F., Hamburger, R.O., et al. "Probabilistic basis for 2000 SAC Federal Emergency Management Agency steel moment frame guidelines", *Journal of Structural Engineering*, **128**(4), pp. 526–533 (2002).
4. Mackie, K. and Stojadinovic, B. "Probabilistic seismic demand model for California highway bridges", *Journal of Structural Engineering*, **6**(6), pp. 428–481 (2001).
5. Mashayekhi, M.R., Harati, M., Barmchi M., et al. "Introducing a response-based duration metric and its correlation with structural damages", *Bulletin of Earthquake Engineering*, **17**, pp. 5987–6008 (2019).
6. Mashayekhi, M.R., Harati, M., Darzi, A., et al. "Incorporation of strong motion duration in incremental-based seismic assessments", *Engineering Structures*, **223**, pp. 111–144 (2020).
7. Nielson, B.G. "Analytical fragility curves for highway bridges in moderate seismic zones", Ph.D. Thesis, Georgia Institute of Technology, Atlanta (2005).
8. Ramanathan, K.N. "Next generation seismic fragility curves for California bridges incorporating the evolution in seismic design philosophy", Ph.D. Thesis, Georgia Institute of Technology, Atlanta (2012).
9. Shinozuka, M., Feng, M.Q., Lee, J., et al. "Statistical analysis of fragility curves", *Journal of Engineering Mechanics*, **126**(12), pp. 1224–1231 (2000).
10. Pan, Y., Agrawal, A.K., and Ghosn, M. "Seismic fragility of continuous steel highway bridges in New York state", *Journal of Bridge Engineering*, **12**(6), pp. 689–699 (2007).
11. Padgett, J.E. and DesRoches, R. "Methodology for the development of analytical fragility curves for retrofitted bridges", *Earthquake Engineering and Structural Dynamics*, **37**(8), pp. 1157–1174 (2008).
12. Pourzeynali S. and Hosseinnezahd A. "Reliability analysis of bridge structures for earthquake excitations", *Scientia Iranica*, **16**(1), pp. 1–15 (2009).
13. Basöz, N.I., Kiremidjian, A.S., King, S.A., et al. "Statistical analysis of bridge damage data from the 1994 Northridge, CA, earthquake", *Earthquake Spectra*, **15**(1), pp. 25–54 (1999).
14. De Grandis, S.D., Domaneschi, M., and Perotti, F. "A numerical procedure for computing the fragility of NPP components under random seismic excitation", *Nuclear Engineering and Design*, **239**(11), pp. 2491–2499 (2009).
15. Perotti, F., Domaneschi, M., and De Grandis, S.D. "The numerical computation of seismic fragility of base-isolated nuclear power plants buildings", *Nuclear Engineering and Design*, **262**, pp. 189–200 (2013).
16. Vasseghi, A., Bahrani, M.K., and Soltani, M. "Seismic retrofit of a typical reinforced concrete bridge bent in Iran", *Scientia Iranica*, **22**(4), pp. 1402–1410 (2015).
17. Hojat Jalali, H. and Maleki, S. "Nonlinear behavior of concrete end diaphragms in straight slab-girder bridges", *Scientia Iranica*, **22**(3), pp. 604–614 (2015).
18. Sotoudeh, M.A., Ghaemian, A., and Sarvghad, Moghadam A. "Determination of limit-states for near-fault seismic fragility assessment of concrete gravity dams", *Scientia Iranica*, **22**(3), pp. 1135–1155 (2019).
19. Ghaffari, E., Estekanchi, H.E., and Vafai, A. "Application of endurance time method in seismic analysis of bridges", *Scientia Iranica*, **27**(4), pp. 1751–1761 (2020).
20. Barnawi, W.T., and Dyke, S.J. "Seismic fragility relationships of a cable-stayed bridge equipped with response modification systems", *Journal of Bridge Engineering*, **19**(8), pp. 1–12 (2014).

21. Mangalathu, S., Choi, E., Park, H.C., et al. "Probabilistic seismic vulnerability assessment of tall horizontally curved concrete bridges in California", *Journal of Performance of Constructed Facilities*, **32**(6), pp. 1–11 (2018).

22. Xie, Y. and DesRoches, R. "Sensitivity of seismic demands and fragility estimates of a typical California highway bridge to uncertainties in its soil-structure interaction modeling", *Engineering Structures*, **189**, pp. 605–617 (2019).

23. Noori, H.R., Memarpour, M.M., and Soltanieh, M.Y. "Effects of ground motion directionality on seismic behavior of skewed bridges considering SSI", *Soil Dynamics and Earthquake Engineering*, **127**, p. 105820 (2019).

24. Chen, X. "System fragility assessment of tall-pier bridges subjected to near-fault ground motions", *Journal of Bridge Engineering*, **25**(3), pp. 1–12 (2020).

25. Shekhar, S., Ghosh, J., and Ghosh, S. "Impact of design code evolution on failure mechanism and seismic fragility of highway bridge piers", *Journal of Bridge Engineering*, **25**(2), pp. 1–19 (2020).

26. Wei, B., Zhuo, Y., Hu, Z., et al. "Influence of site conditions on structural vulnerability of a super high three-tower cable-stayed bridge", *Structures*, **34**, pp. 3882–3893 (2021).

27. Rachedi, M., Matallah, M., and Kotronis, P. "Seismic behavior & risk assessment of an existing bridge considering soil-structure interaction using artificial neural networks", *Engineering Structures*, **232**, p. 111800 (2021).

28. Salimi, M.R., Afsar Dizaj, E., and Kashani, M.M. "Fragility analysis of rectangular and circular reinforced concrete columns under bidirectional multiple excitations", *Engineering Structures*, **233**, p. 111887 (2021).

29. Todorov, B. and Muntasir Billah, A.H.M. "Seismic fragility and damage assessment of reinforced concrete bridge pier under long-duration, near-fault, and far-field ground motions", *Structures*, **31**, pp. 671–685 (2021).

30. Fosoul Saber, A.S. and Tait Michael, J. "Soil-pile-structure interaction effects on seismic demands and fragility estimates of a typical Ontario highway bridge retrofitted with fiber reinforced elastomeric isolator", *Soil Dynamics and Earthquake Engineering*, **151**, p. 106967 (2021).

31. Zanardo, G., Hao, H., and Modena, C. "Seismic response of multi-span simply supported bridges to a spatially varying earthquake ground motion", *Earthquake Engineering and Structural Dynamics*, **31**(6) (2002).

32. Yu, M., Erlei, Y., Bin, R., et al. "Improved Hilbert spectral representation method and its application to seismic analysis of shield tunnel subjected to spatially correlated ground motions", *Soil Dynamics and Earthquake Engineering*, **111**, pp. 119–130 (2018).

33. Papadopoulos, S.P. and Sextos, A.G. "Anti-symmetric mode excitation and seismic response of base-isolated bridges under asynchronous input motion", *Soil Dynamics and Earthquake Engineering*, **113**, pp. 148–161 (2018).

34. Papadopoulos, S.P. and Sextos, A.G. "Simplified design of bridges for multiple-support earthquake excitation", *Soil Dynamics and Earthquake Engineering*, **113**, p. 106013 (2020).

35. Yao, E., Wang, S., Ruan, B., et al. "Numerical study on site response considering ground motion spatial variation", *Soil Dynamics and Earthquake Engineering*, **127**, p. 105836 (2019).

36. Yao, E., Wang, S., Miao, Y., et al. "Simulation of fully non-stationary spatially varying ground motions considering nonlinear soil behavior", *Soil Dynamics and Earthquake Engineering*, **129**, p. 105954 (2020).

37. El Haber, E., Cornou, C., Jongmans, D., et al. "Impact of spatial variability of shear wave velocity on the lagged coherency of synthetic surface ground motions", *Soil Dynamics and Earthquake Engineering*, **145**, p. 106689 (2021).

38. McKenna, F., Scott, M.H., and Fenves, G.L. "Nonlinear finite element analysis software architecture using object composition", *Journal of Computing in Civil Engineering*, **24**(1), pp. 95–107 (2010).

39. Konakli, A. and Der Kiureghian, A., *Stochastic Dynamic Analysis of Bridges Subjected to Spatially Varying Ground Motions*, Pacific Earthquake Engineering Research Center, University of California, Berkeley, CA (2011).

40. Konakli, K. and Der Kiureghian, A. "Simulation of spatially varying ground motions including incoherence, wave-passage and differential site-response effects", *Earthquake Engineering and Structural Dynamics*, **41**(3), pp. 495–513 (2012).

41. Liao, S. and Zerva, A. "Physically compliant, conditionally simulated spatially variable seismic ground motions for performance-based design", *Earthquake Engineering and Structural Dynamics*, **35**(7), pp. 891–919 (2006).

42. Der Kiureghian, A. "A coherency model for spatially varying ground motions", *Earthquake Engineering and Structural Dynamics*, **25**(1), pp. 99–111 (1996).

43. Luco, J.E. and Wong, H.L. "Response of a rigid foundation to a spatially random ground motion", *Earthquake Engineering and Structural Dynamics*, **14**(6), pp. 891–908 (1986).

44. Bi, K.M., Hao, H., and Chouw, N. "Influence of ground motion spatial variation, site condition and SSI on the required separation distances of bridge structures to avoid seismic pounding", *Earthquake Engineering and Structural Dynamics*, **40**(9), pp. 1027–1043 (2011).

45. Soyluk, K. and Dumanoglu, A. "Spatial variability effects of ground motions on cable-stayed bridges", *Soil Dynamics and Earthquake Engineering*, **24**(3), pp. 241–250 (2004).

46. Der Kiureghian, A. and Neuenhofer, A. "Response spectrum method for multi-support seismic excitations", *Earthquake Engineering and Structural Dynamics*, **21**(8), pp. 713–740 (1992).

47. Ketchum, M., Chang, V., and Shantz, T., *Influence of Design Ground Motion Level on Highway Bridge Costs*, Pacific Earthquake Engineering Research Center, University of California Berkeley CA (2004).

48. Taucer, F., Spacone, E., and Filippou, F.C., *A Fiber Beam-Column Element for Seismic Response Analysis of Reinforced Concrete Structures*, Earthquake Engineering Research Center, College of Engineering, University of California, Berkeley (1991).

49. Mander, J., Priestly, M., and Park, R. "Theoretical stress-strain model for confined concrete", *Journal of Structural Engineering*, **114**(8), pp. 1804–1826 (1988).

50. Zhang, J. and Markis, N. "Seismic response analysis of highway overcrossings including soil-structure interaction", *Earthquake Engineering & Structural Dynamics*, **31**(11), pp. 1967–1991 (2002).

51. Medina, R.A. and Krawinkler, H., *Seismic Demands for Non-Deteriorating Frame Structures and Their Dependence on Ground Motions*, John, A., Blume, Earthquake Engineering Center, Stanford University, Stanford, CA (2003).

52. Ghobarah, A. "Performance-based design in earthquake engineering: state of development", *Engineering Structures*, **23**(8), pp. 878–884 (2001).

53. Wolf, J. "Spring-dashpot-mass modeling for foundation vibrations", *Earthquake Engineering and Structural Dynamics*, **26**(9), pp. 931–949 (1997).

54. Vamvatiskos, D. and Cornell, C. "Incremental dynamic analysis", *Earthquake Engineering and Structural Dynamics*, **31**(3), pp. 491–514 (2002).

Biographies

Aziz Hosseinnezhad is a PhD candidate at the Civil Engineering Department of the University of Mohaghegh Ardabili, Ardabil, Iran. He received his BS degree in Civil Engineering from KNT University of Technology and his MS degree in Structural Engineering at the University of Guilan. His research interests include work on the seismic behavior of long-span bridges under non-uniform excitations, the non-linear behavior of structures, soil-structure interactions, incremental dynamic analysis, and fragility assessments. He is a professional engineer in the field of structural designing of reinforced concrete and steel building.

Amin Gholizad is a Professor at the Civil Engineering Department of the University of Mohaghegh Ardabili, Ardabil, Iran. He received all his degrees at Sharif University of Technology and in 2009, graduated as a PhD in Structural Engineering. He has supervised a large number of MS and PhDs students. He is currently the Head of the Faculty of Engineering. His current research activities include reliability engineering, seismic control, fatigue, health monitoring, random vibration, analysis and design of coastal structures, and dynamic response of structures under non-uniform excitations.